Front. Mech. Eng. 2019, 14(1): 65–75
https://doi.org/10.1007/s11465-018-0520-z

RESEARCH ARTICLE

Mao LI, Yuanzhi LIU, Xiaobang WANG, Jie ZHANG

Modeling and optimization of an enhanced battery thermal management system in electric vehicles

Abstract This paper models and optimizes an air-based battery thermal management system (BTMS) in a battery module with 36 battery lithium-ion cells. A design of experiments is performed to study the effects of three key parameters (i.e., mass flow rate of cooling air, heat flux from the battery cell to the cooling air, and passage spacing size) on the battery thermal performance. Three metrics are used to evaluate the BTMS thermal performance, including (i) the maximum temperature in the battery module, (ii) the temperature uniformity in the battery module, and (iii) the pressure drop. It is found that (i) increasing the total mass flow rate may result in a more non-uniform distribution of the passage mass flow rate among passages, and (ii) a large passage spacing size may worsen the temperature uniformity on the battery walls. Optimization is also performed to optimize the passage spacing size. Results show that the maximum temperature difference of the cooling air in passages is reduced from 23.9 K to 2.1 K by 91.2%, and the maximum temperature difference among the battery cells is reduced from 25.7 K to 6.4 K by 75.1%.

Keywords thermal management, electric vehicle, lithium-ion battery, temperature uniformity, design optimization

Received October 26, 2017; accepted February 26, 2018

Mao LI, Yuanzhi LIU, Xiaobang WANG, Jie ZHANG (✉)
Department of Mechanical Engineering, The University of Texas at Dallas, Richardson, TX 75080, USA
E-mail: jiezhang@utdallas.edu

Mao LI
Beijing Institute of Aerospace Testing Technology, Beijing 100074, China

Xiaobang WANG
School of Mechanical Engineering, Dalian University of Technology, Dalian 116024, China

1 Introduction

Electric vehicles (EVs) are powered by a large number of battery cells. Among all battery technologies, lithium-ion battery is becoming to be the energy storage of choice for EVs and is expected to be widely used in the coming years. However, due to the narrow range of the optimal operating temperature, the development is restricted by the safety issues and the long cycle life of the lithium-ion batteries [1,2]. Thermal management plays a significant role in the life, performance, safety, and cost of the lithium-ion battery modules in the EVs [3–6]. Aiming to enhance the battery performance by improving the thermal environment for batteries, many cooling schemes, such as air-based systems, liquid-based systems, phase change material-based systems, heat pipe based-systems, and hybrid systems, have been developed for battery thermal management systems (BTMS) [7–16]. The BTMS aims to improve the temperature uniformity among all battery cells, and to prevent battery cells from very high temperature that may likely cause their explosion.

The air-based BTMS has been widely applied in EVs due to its low cost, simple structure, and light weight. Various methods have been developed in the literature to study the air-based BTMS, including numerical simulations, experiments, and optimization. The approaches to improve the temperature uniformity are also varying. Most of the existing work in air-based BTMS focuses on the cooling channel design and optimization. For example, Park [7] simulated the cooling performance with different types of air ventilation, and found that the cooling performance was significantly improved by adding an extra ventilation. Basu et al. [17] used a coupled three-dimensional electrochemical thermal model to evaluate the effects of coolant flow rate and discharge current on the pack temperature. Hwang et al. [18] built a computational fluid dynamics (CFD) model of an air-based BTMS, and found that the locations and shapes of the air inlet and outlet had significant impacts on the heat dissipation. Fan et al. [19] studied the effects of gap spacing and air flow

rate on the cooling performance, and found that one-side cooling and uneven gap spacing could improve the temperature uniformity. Zhao et al. [20] established air cooling models for a cylindrical lithium-ion power battery pack to study the thermal management performance with different parameters, such as ventilation type and velocity, gap spacing between battery cells, the temperature of environment and air, number of single row cells, and battery dimension. Xun et al. [21] developed numerical models of BTMS to analyze the impacts of the volume ratio and the size of the cooling channel, and found that a larger channel could improve the evenness of the temperature distribution and the energy efficiency. Ji et al. [22] proposed an active temperature control method by optimally arranging battery cells and controlling the coolant flow rate to equalize the temperature distribution of the battery cells.

Other work focused on adding auxiliary components to enhance the heat transfer for air-based BTMS. For example, Sun et al. [23,24] developed a transient battery thermal model and proposed a Z-type (the inlet and outlet are located on opposite sides) air-cooled battery pack with taper manifold, cooling plate, and corrugations to improve the battery temperature uniformity. Mohammadian and Zhang [25] embedded metal foam and pin-fin heat sinks to an air-cooled battery to enhance the thermal performance. Ling et al. [26] coupled phase change material and forced-air cooling in their BTMS design.

However, most of the existing studies have not comprehensively analyzed the effects of the key design parameters on the air-based BTMS performance, which could potentially be used to optimize the BTMS design. To bridge this gap in air-based BTMS design, this paper focuses on investigating the effects of key design parameters on the thermal performance of an air-based BTMS, and optimizing these key design parameters. In this paper, the influence of three key parameters, including the mass flow rate of the cooling air, the heat flux on the battery cell wall, and the passage spacing size between the adjacent battery cells, are modeled, simulated, and analyzed. In addition, an optimization strategy is developed based on the parametric study to improve the thermal performance of the BTMS.

The remainder of the paper is organized as follows. Section 2 describes the modeling and numerical methods of the air-based BTMS; a sensitivity analysis of key BTMS parameters is performed in Section 3; Section 4 discusses the BTMS optimization results; concluding remarks and future work are provided in Section 5.

2 Modeling and numerical methods

2.1 Battery model

A U-type battery module scheme with 36 battery cells and 37 cooling passages was established in this work, in which the inlet and outlet are located on the same side, as shown in Fig. 1. The width, thickness, and height of the battery cells are 65, 16, and 151 mm, respectively. The heights of both the inlet manifold and the outlet manifold are 20 mm. The inlet and outlet are on the same side of the battery module. The cooling air comes through the inlet manifold and then enters into the passages between the adjacent battery cells, and converges in the outlet manifold to flow out. The passages and battery cells are numerically labeled for the sake of analysis. The passage/battery cell next to the module inlet/outlet is numbered 1. The battery model is built according to Park's work [7]. The work in our paper focuses on modeling and analyzing the flow characteristics of the cooling air on the performance of the battery module. The electro-chemical modeling and the heat

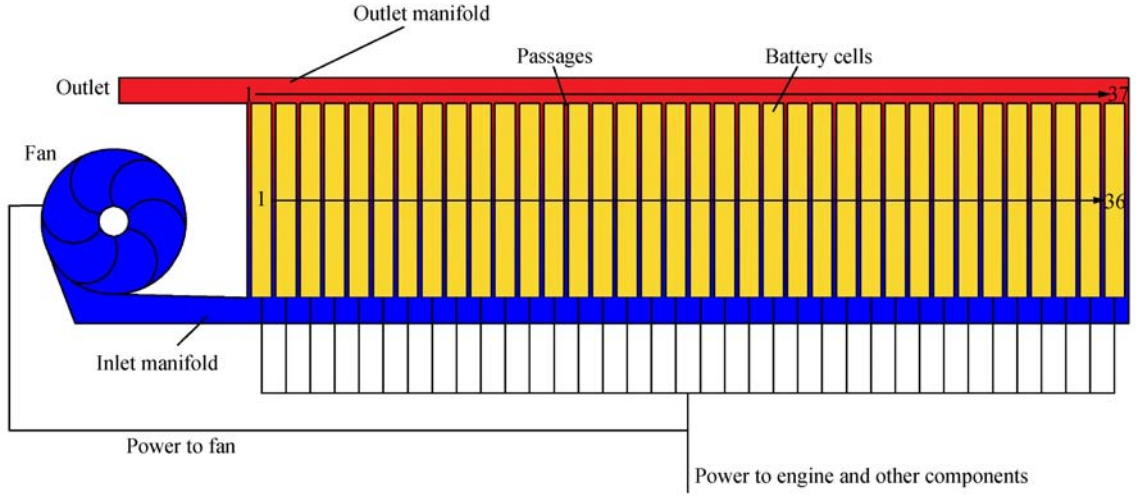

Fig. 1 Battery module model

generation modeling in the battery cells are not within the scope of this paper. The heat generated by the battery cells is replaced by the heat flux that can be set on the battery cell wall. The characteristics of the fan (that is used to supply the cooling air) are not taken into account either. A mass flow rate boundary condition is applied to the air inlet.

2.2 Parameters selection

During the battery charging and discharging processes of the battery, the heat is generated by electro-chemical reactions. If the heat could not be dissipated timely, the accumulation of heat would lead to an excessive high temperature in the battery cells, which may shorten the life cycle and even cause safety issues in EVs. In an air-based BTMS, the heat is taken away by the cooling air. The heat exchange between the battery cell walls and the cooling air is modeled by Eqs. (1) and (2).

$$q = h(T_{\mathrm{w}} - T_{\mathrm{a}}), \tag{1}$$

$$\dot{q} = q/A, \tag{2}$$

where q is the heat power, h is the convection heat transfer coefficient, T_{w} is the temperature of the battery cell wall, T_{a} is the temperature of the cooling air near the wall, $\dot{q}$ is the heat flux, and A is the area of the battery cell. T_{w} represents the thermal environment of the battery cell. One of the objectives of the BTMS is to ensure T_{w} within an optimal range. For a certain battery cell, it is seen from Eqs. (1) and (2) that T_{w} is affected by $\dot{q}$, h, and T_{a}.

The cooling air absorbs the heat from the battery cell and the air temperature increases. The correlation between the temperature difference of the cooling air and the heat is modeled by

$$q = c_p \dot{m} \Delta T_{\mathrm{a}}, \tag{3}$$

$$\Delta T_{\mathrm{a}} = T_{\mathrm{in}} - T_{\mathrm{out}}, \tag{4}$$

where c_p is the specific heat at a constant pressure, which is assumed to be a constant if the pressure does not change significantly, $\dot{m}$ is the mass flow rate of the cooling air, ΔT_{a} is the temperature difference of the cooling air, T_{in} and T_{out} are the temperatures of the cooling air at the passage inlet and outlet, respectively.

As seen from Eq. (3), increasing the amount of the cooling air can lower the air temperature difference, i.e., T_{out} is decreased by the increasing $\dot{m}$ with a certain cooling air temperature. Though a low T_{out} does not necessarily ensure a low temperature of the cooling air near the wall T_{a}, it is expected to significantly affect T_{a} and may enhance the thermal performance. In addition, according to Eq. (5), the velocity of the cooling air is increased with the rise of the mass flow rate.

$$\dot{m} = \rho v A_{\mathrm{f}}, \tag{5}$$

where ρ and v are the density and velocity of the cooling air, respectively, and A_{f} is the flow area.

A high velocity magnitude of the fluid near the wall enhances the forced convection heat exchange. However, the high velocity magnitude by increasing $\dot{m}$ also leads to a large pressure drop, thereby resulting in a large power consumption from the battery cell to drive the fan. The relationship between the total pressure, the total temperature, the velocity, and the power of the fan [19] are formulated in Eqs. (6)–(9).

$$\frac{\mathrm{d}p^*}{p^*} = -\frac{kMa^2}{2}\frac{\mathrm{d}T^*}{T^*}, \tag{6}$$

$$Ma = \frac{v}{c}, \tag{7}$$

$$\Delta p = p^*_{\mathrm{in}} - p^*_{\mathrm{out}}, \tag{8}$$

$$P = \Delta p \frac{\dot{m}}{\rho \eta}, \tag{9}$$

where p^* and T^* are the total pressure and total temperature of the cooling air, respectively, k is the specific heat ratio at a constant pressure, M_a is Mach number, c is the local sonic speed, Δp, p^*_{in}, and p^*_{out} are the pressure drop, total pressure at the inlet, and total pressure at the outlet, respectively, P is the fan power, and η is the efficiency of the fan.

Based on Eq. (5), the velocity also increases when the flow area decreases. Because the width of the battery cell is a constant, the flow area changes with the passage spacing size between the adjacent battery cells, as shown in Eq. (10).

$$A_{\mathrm{f}} = bL, \tag{10}$$

where b is the passage spacing size between the adjacent battery cells, and L is the width of the battery cell.

In this study, the mass flow rate of the cooling air ($\dot{m}$), the heat flux from the battery cell to the cooling air ($\dot{q}$), and the passage spacing size (b) are selected as key parameters to analyze their effects on the thermal performance. A design of experiments has been performed to study the effects of these three key parameters on the battery thermal performance. Each parameter is divided into 5 levels, as shown in Table 1. Three groups of numerical simulations are designed, including the mass flow rate group, heat flux group, and passage spacing size group. Benchmark values of the mass flow rate, heat flux, and passage spacing size are 0.0225 kg/s, 245 W/m^2, and 3 mm, respectively. According to Park's work [7], the heating power is 4.8 W per battery cell (i.e., 30625 W/m^3), which can also be validated by another study in Ref. [11]. Note that the spacing size between any two battery cells is even. In the parametric analysis of any individual parameter, the other

Table 1 A design of experiments for the three key parameters

Level	m/(kg·s^{-1})	q/(W·m^{-2})	b/mm
1	0.0175	220	2.0
2	0.0200	245	2.5
3	0.0225	275	3.0
4	0.0250	295	3.5
5	0.0275	320	4.0

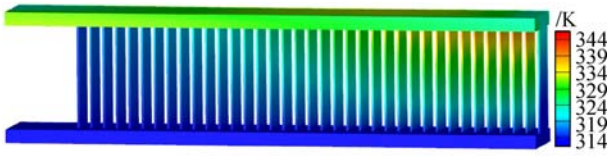

Fig. 2 The temperature distribution of the cooling air

two parameters are assigned with the benchmark values. Due to the different passage spacing sizes, the total lengths of the battery modules are different in the passage spacing size group; while the total length is a constant in the mass flow rate group and the heat flux group.

The metrics used to evaluate the BTMS thermal performance are: (i) The maximum temperature in the battery module, (ii) the temperature uniformity in the battery module, and (iii) the pressure drop. In addition, the effects of the three parameters on the passage mass flow rate are also analyzed, due to its importance on the distribution of the velocity and the cooling air temperature.

The commercial software FLUENT 17.0 is used in the work. The shear-stress transport (SST) turbulence model [7,19,27] and the SIMPLEC method are selected to solve the simulations based on the steady and pressure-based solver. The second order upwind is used to disperse the pressure, density, and momentum equations. The thermal radiation transfer is assumed to be negligible in the work. The grid cells of the battery module are about 2400000 after testing several grid densities. The boundary condition types are listed in Table 2. The temperature of the cooling air at the inlet is set to 313 K and the pressure at the outlet is set to 101325 Pa in all simulations. Figure 2 shows one of the CFD study cases.

Table 2 Boundary condition types

Boundary	Type
Air inlet	Mass flow rate inlet
Air outlet	Pressure outlet
Battery cell wall	Wall with heat flux
Battery module wall	Adiabatic and no-slip wall

3 Sensitivity analysis of key parameters

3.1 Effects of the mass flow rate

Figure 3 shows the effects of the mass flow rate on the maximum temperature difference (ΔT_{max}) and pressure drop (Δp), the maximum temperature on the battery cell, and passage mass flow rate in the battery module. It is seen from Fig. 3(a) that as the mass flow rate increases from 0.0175 to 0.0275 kg/s, the temperature difference decreases from 33.2 K to 26.3 K by 20.8%, and the pressure drop increases from 112.5 to 252.2 Pa by 124.2%. According to Eq. (9), due to the increase of both the mass flow rate and the pressure drop, the power consumption of the cooling system in the case of 0.0275 kg/s is approximately 3.5 times of that in the case of 0.0175 kg/s. Thus, improving the thermal performance by increasing the mass flow rate will significantly increase the energy consumption.

In the battery module, the maximum temperature on the battery cell increases from the first battery cell to the last battery cell, as shown in Fig. 3(b). The maximum temperature difference among the battery cells is over 20 K for all cases. Generally, the pressure of the cooling air decreases along the flow direction. In this module, because the air inlet and outlet are on the same side, from the first passage to the last passage, the pressure of the cooling air falls in the inlet manifold and rises in the outlet manifold, which indicates that the pressure difference between the passage inlet and outlet decreases. This smaller pressure difference causes less air to flow through the passage, and thereby the passage mass flow rate decreases as shown in Fig. 3(c). According to Eq. (3), due to the decreasing passage mass flow rate, the air temperature increases. As a result, the maximum temperature on the battery cell rises as well.

Moreover, with a higher mass flow rate, a larger passage mass flow rate in the front passages is observed in Fig. 3(c), while it is more stable in the rear passages. This means the distribution of the passage mass flow rate becomes more uneven when increasing the cooling air, and most of the increased air only flows through the front passages. In addition, it is seen from Fig. 3(b) that the maximum temperature on the battery cell in the front part of the battery module decreases much less than that in the rear part. This indicates that the maximum temperature on the battery cell is relatively more sensitive to the passage mass flow rate in the rear part of the battery module than that in the front part of the battery module. This suggests that increasing the passage mass flow rate in the rear passages will reduce the maximum temperature on the battery cell, and the distribution of the temperature among all battery cells will become more even. Thus in this paper, an approach is developed to redistribute the cooling air, which will be discussed in Section 4.

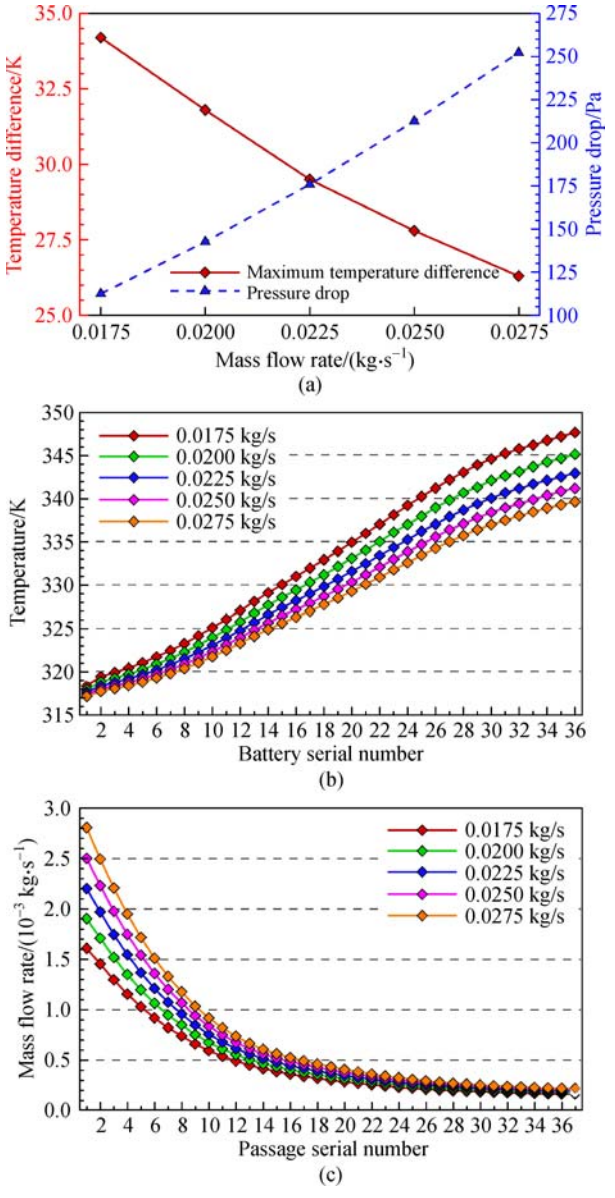

Fig. 3 Effects of mass flow rates on the (a) maximum temperature difference and pressure drop, (b) maximum temperature on the battery cell, and (c) passage mass flow rate

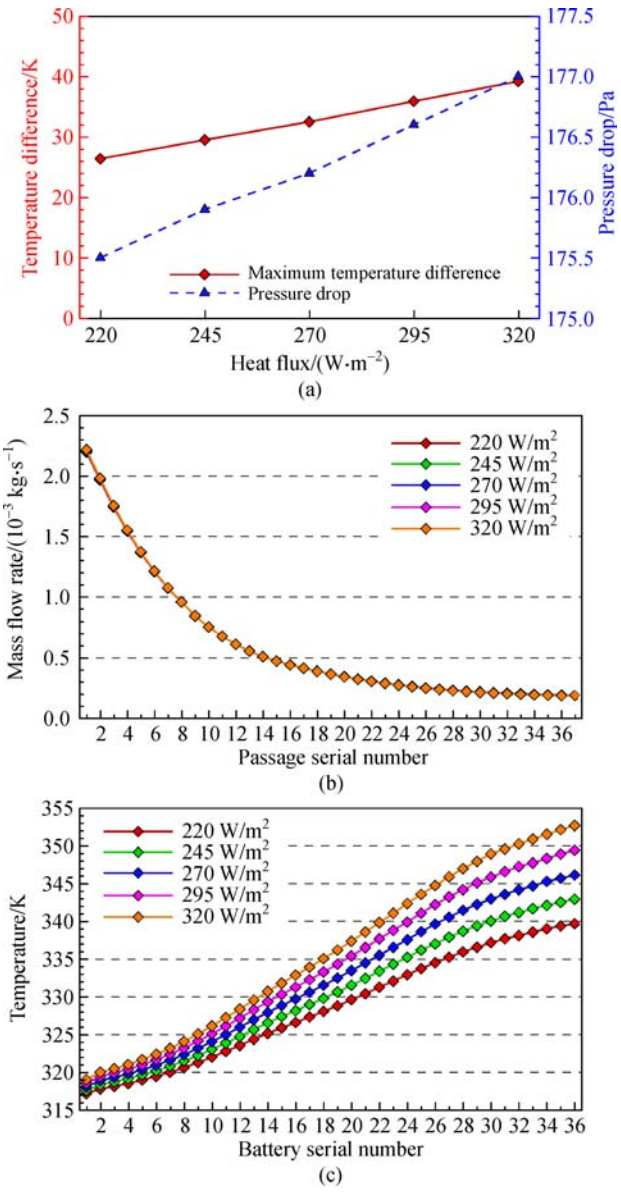

Fig. 4 Effects of the heat flux on the (a) maximum temperature difference and pressure drop, (b) passage mass flow rate, and (c) maximum temperature on the battery cell

3.2 Effects of the heat flux

Figure 4(a) shows the effects of heat flux to the maximum temperature difference and the pressure drop. As the heat flux increases from 220 to 320 W/m^2, the maximum temperature difference increases by 13 K approximately, while the pressure drop only increases by about 1.5 Pa. For a constant mass flow rate, the cooling air needs to take away more heat with a larger heat flux, which may cause a higher air temperature and a worse thermal environment. Though a higher temperature leads to a lower density of the cooling air, it does not affect the distributions of the passage mass flow rate, as shown in Fig. 4(b). The values of the passage mass flow rate are almost identical in the same passage with different heat fluxes.

As the heat flux increases from 220 to 320 W/m^2, both the maximum temperature of the battery cell and the outlet air temperature increase noticeably, as shown in Fig. 4(c). The temperatures of the rear passages, in particular, are higher than that of the front passages. For instance, at the last passage, where the passage mass flow rate is 0.0002 kg/s, the maximum temperature on the last battery cell increases by approximately 13 K. In contrast, the maximum temperature on the first battery cell increases by about 2 K where the passage mass flow rate is about 0.0022 kg/s in the first passage. This finding shows that increasing the heat flux may reduce the temperature uniformity within the battery module.

3.3 Effects of the passage spacing size

With different passage spacing sizes, the maximum temperature difference and pressure drop, maximum temperature on the battery cell, and passage mass flow rate in the battery module, are illustrated in Fig. 5. It is seen from Fig. 5(a) that the maximum temperature difference increases rapidly as the passage spacing size increases, which means the thermal performance is deteriorated. For example, when the passage spacing size is 2.0 mm, the maximum temperature difference is about 15 K; when the passage spacing size is 4.0 mm, the maximum temperature difference is increased by approximately 44 K. The maximum temperature on the battery cell occurs at the last battery cell, as shown in Fig. 5(b). It is found that the passage spacing size significantly affects the temperature uniformity. When increasing the passage spacing size, the maximum temperature on the battery cell decreases slightly at the front battery cells, and increases dramatically at the rear battery cells, which enlarges the temperature difference. In addition, with the same increment of the passage spacing size, a large increment of the maximum temperature on the battery cell is observed in the cases of the large passage spacing size. According to Eqs. (1) and (3), the temperature on the battery cell is highly correlated with the passage mass flow rate. From the distribution of the passage mass flow rate with different passage spacing sizes in Fig. 5(c), it is seen that the passage mass flow rate increases in the front passages and decreases in the rear passages as the passage spacing size increases. Thus, the uneven distribution of the passage mass flow rate leads to a higher temperature difference in the case of larger passage spacing sizes.

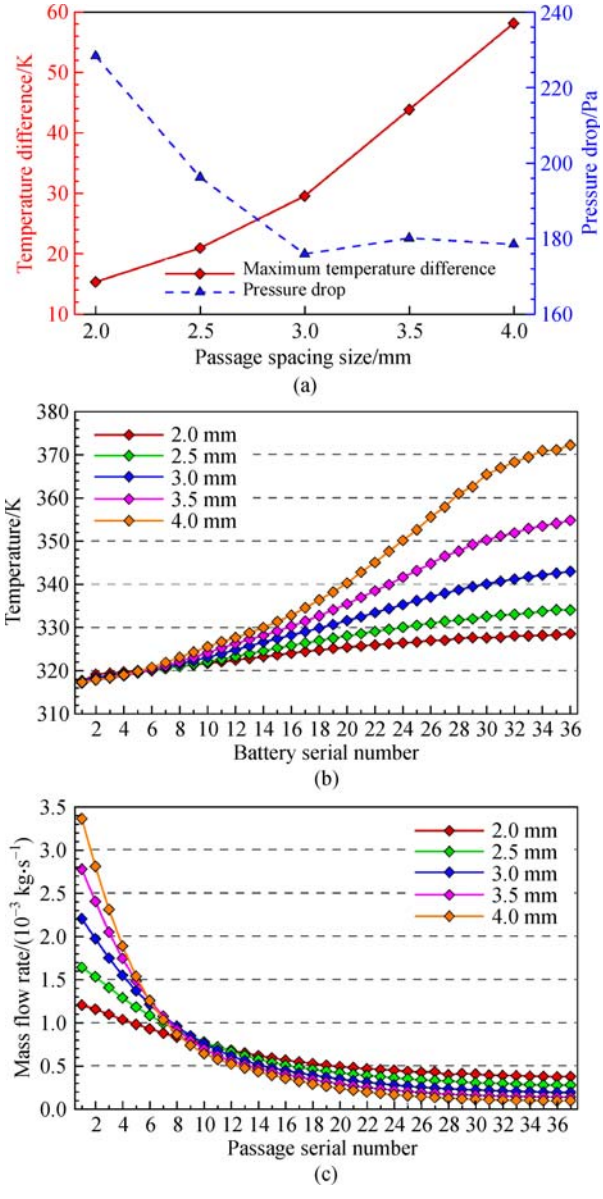

Fig. 5 Effects of the passage spacing size on the (a) maximum temperature difference and pressure drop, (b) maximum temperature on the battery cell, and (c) passage mass flow rate

Moreover, there is over 50% of the cooling air that flows through the front six passages, when the passage spacing sizes are larger than 3.0 mm. Since the total mass flow rate is fixed, the amount of the cooling air that flows through the rear passages reduces remarkably, and therefore the air temperature increases dramatically.

Nevertheless, the pressure drop between the air inlet and outlet does not decrease continuously when the spacing size increases. In Fig. 5(a), the pressure drop between the air inlet and outlet decreases from about 225 to 180 Pa, when the passage spacing size increases from 2.0 to 3.0 mm; and the pressure drop is stable when the passage spacing size changes from 3.0 to 4.0 mm. For each passage, the pressure drop between the air inlet and outlet consists of three parts: The pressure drop from the air inlet to the passage inlet (Δp_{in}), the pressure drop from the passage inlet to the passage outlet (Δp_{p}), and the pressure drop from the passage outlet to the air outlet (Δp_{out}). The first passage is used as an example to analyze the pressure drop. At the first passage, Δp_{in} and Δp_{out} are almost the same among all the cases due to the same mass flow rate and the same dimension of the manifold. Thus, the pressure drop between the air inlet and outlet mainly depends on Δp_{p}. Generally, the pressure drop decreases when the flow area increases. When the passage size is relatively small, the pressure drop is much sensitive to the passage size change due to the boundary layer effect. Figure 6(a) shows a mid-plane velocity distribution that is extracted from the first passage with different spacing sizes. It is found that the thickness of the boundary layer almost occupies the whole passage in the cases of 2.0 and 2.5 mm, and thus a large pressure drop is caused (as seen in Fig. 6(b)). When the passage spacing size is larger than 3.0 mm, the boundary layer effect is reduced. Therefore, a small difference of the passage pressure drop is observed in Fig. 6(b) with a large passage spacing size.

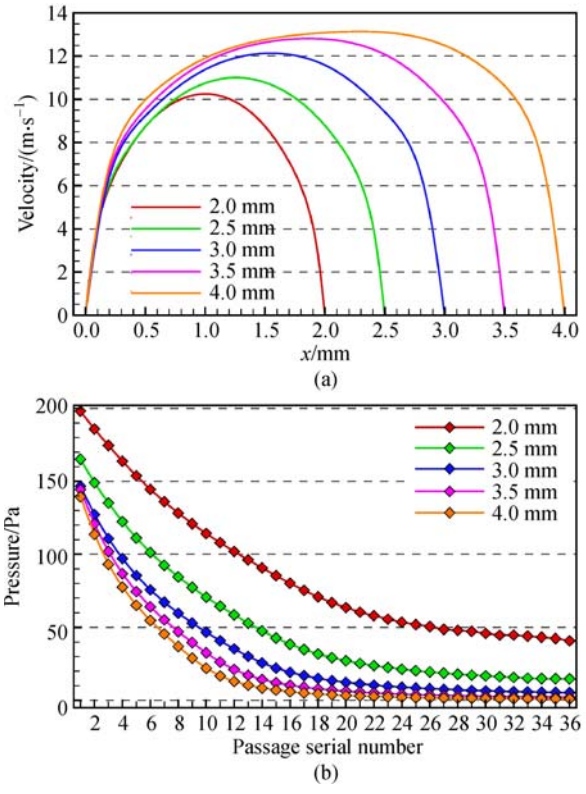

Fig. 6 Distributions of the (a) velocity on the mid-plane in the first passage, and (b) passage pressure drop with different passage spacing sizes

4 Thermal management system optimization

4.1 Optimization methodology

From the parametric analysis of the mass flow rate, the heat flux, and the passage spacing size on the thermal performance, it is found that the temperature distribution among the battery cells is not even within the battery module. In all cases discussed in Section 3, it is found that even we change the three key parameters in a large range, the temperatures on the rear battery cells are still larger than those on the front battery cells. However, the temperature uniformity over a single battery cell, as well as the whole battery module, has a great impact on the capacity and shorten cycle life. Extensive studies [11,28,29] have shown that a high temperature will accelerate the degradation of the capacity and shorten the cycle life. The temperature uniformity of a single battery cell is affected by its intrinsic properties, such as electrode and electrolyte materials, thermal conductivity, battery dimensions, and extrinsic factors like convection heat transfer coefficient and media. The temperature uniformity of a battery module is affected by the passage spacing size, cooling air, manifold configuration, and others.

As previously discussed, due to the heat taken away by the cooling air, the cooling air temperature that inversely correlates to the mass flow rate plays an important role in the temperature on the battery cell. According to the parametric analysis in Section 3, in the battery module with even spacing size passages, the different pressure differences among the passages lead to an uneven distribution of the passage mass flow rate. Thereby, the temperatures on the battery cell are uneven. To reduce the impacts of the pressure drop in the manifold on the passage pressure difference, a significant amount of work has been done in the literature by using taper manifold or changeable inlet and outlet [7,23,24,30]. However, due to the pressure drop in the manifold, it is challenging to eliminate the pressure difference when the inlet and outlet of the battery module are on the same side. In addition to the pressure difference, the flow area of each passage is another factor that largely affects the distribution of the passage mass flow rate. Thus in this study, the passage spacing size is selected as a design variable for optimizing the battery module. The designed optimal passage spacing size will be varying among different passages. Note that the convection heat transfer coefficient (h) is another important parameter that affects the temperature of the battery cell, which is beyond the scope of this paper. In the numerical simulations, the heat transfer process is simulated according to the predefined structure of the battery module, the mass flow rate, the cooling air and others.

In this study, the optimization seeks to improve the temperature uniformity at the module scale. In the passage spacing size optimization, the configuration of the manifolds and the locations of the inlet and outlet are fixed. The mass flow rate, the heat flux, and total length of the battery module are set as constants, i.e., 0.0225 kg/s, 245 W/m^2, and 687 mm, respectively. A 3 mm passage spacing size is selected as the benchmark.

In the simulations, the temperature difference of the cooling air between the outlet and inlet of each passage (ΔT_{ai}) can be extracted. Since the heat flux is assumed to be uniform, if the mass flow rate distribution is balanced, the temperature distribution should be even, and ΔT_{ai} will equal to the air temperature difference (ΔT_a). In practice, due to the uneven temperature distribution, ΔT_{ai} and ΔT_a are different. In this work, the passage spacing size b is modified according to the difference between ΔT_a and ΔT_{ai}. The air temperature difference ΔT_a is used as a target temperature. According to Eqs. (3), (6), and (9), and assuming that the heat is dissipated by cooling air, the relationship between ΔT_a and ΔT_{ai} is described as

$$\rho_{2i} v_{2i} b_{2i} \Delta T_a = \rho_{1i} v_{1i} b_{1i} \Delta T_{ai}, \tag{11}$$

where the subscripts 1 and 2 represent the parameters before and after optimization, respectively, and i is the passage number.

Two approaches are developed for the optimization. In

the first approach, the density and velocity are assumed as constants, and Eq. (11) can be simplified to be Eq. (12). In order to keep the total length of the battery module, the passage spacing size is modified to be Eq. (13). Then the modified spacing size is validated by CFD.

$$b_{2i} = \frac{\Delta T_{\mathrm{a}}}{\Delta T_{\mathrm{a}i}} b_{1i}, \tag{12}$$

$$b'_{2i} = b_{2i} \frac{nb}{\sum_{i=1}^{n} b_{2i}}, \tag{13}$$

where b'_{2i} is the optimized passage spacing size.

In the second approach, ρ_{1i} and v_{1i} are extracted from the CFD simulation results, and ρ_{2i} and v_{2i} are the average values between the air inlet and outlet.

4.2 Optimization results

The passage spacing sizes of the benchmark case (M0) and the optimization case using the first approach (M1) are shown in Fig. 7(a). It is seen that the passage spacing size is increased from 0.5 mm at the first passage to 5.5 mm at the last passage in the M1 case. Figure 7(b) shows the distribution of the maximum temperature on the battery cell for cases of M0 and M1. It is shown that the air temperature at the passage outlet and the maximum temperature on the battery cell in the front part of the battery module in M1 are much higher than those in M0, though they are decreased and become more even in the rear passages. In M1, the maximum temperature on the battery cell is over 420 K. By comparing the passage spacing sizes (Fig. 7(a)) and the temperatures (Fig. 7(b)), both the air temperature at the passage outlet and the maximum temperature on the battery cell in M1 are over 330 K in the first 8 passages; the temperatures are very sensitive to the passage spacing size when it is smaller than 1 mm. From the mass flow rate distribution as shown in Fig. 7(c), the mass flow rates in the front passages in M1 are much smaller than those in M0.

With small passage spacing sizes in the front passages, the velocities are decreased dramatically due to the boundary layer effect. Therefore, the mass flow rates are significantly reduced, resulting in high temperatures in the front passages. This finding suggests that the assumptions of the constant velocity and density by neglecting the boundary layer effect are not practical. In the rear passages, the temperature uniformity is improved, because the effect of the boundary layer is small with large passage sizes.

The distributions of the air temperature at the passage outlet and the maximum temperature on the battery cell by using the second approach are shown in Fig. 8(a). Three cases are simulated, named M2, M3, and M4. The input parameters (ρ, v, b, ΔT_{a}) for the cases of M2, M3, and M4 are from the results of M0, M2, and M3, respectively. Figure 8(b) shows the distribution of the maximum

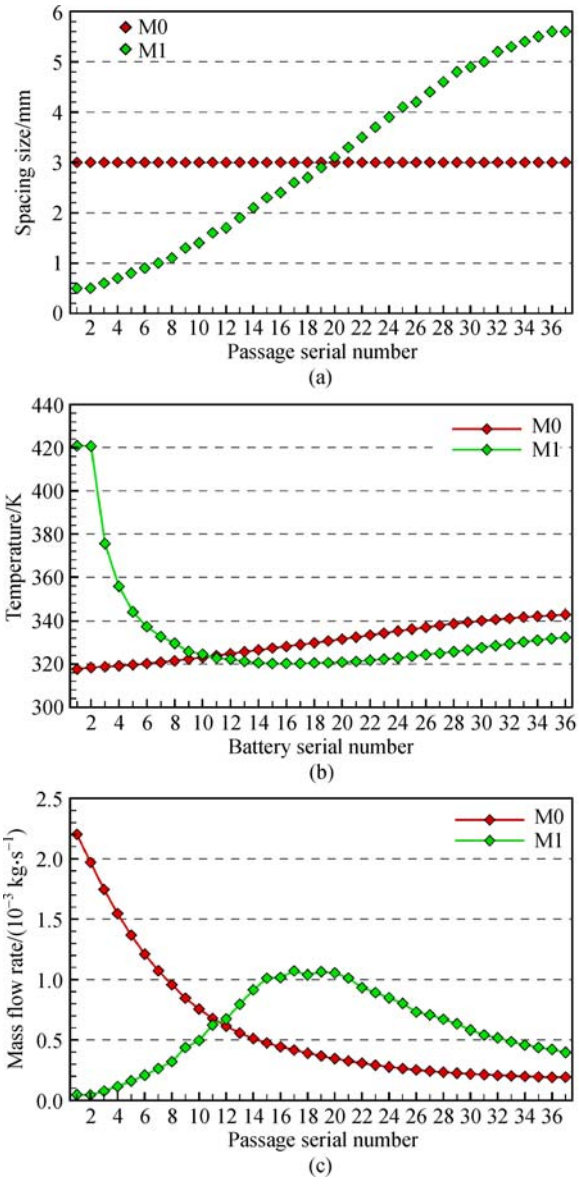

Fig. 7 Distributions of the (a) passage spacing size, (b) maximum temperature on the battery cell, and (c) passage mass flow rate for M0 and M1

temperature on the battery cell for M0, M2, M3, and M4. The maximum temperature difference of the cooling air among the passages ΔT_{amax} and the maximum temperature difference on the battery cells ΔT_{max} are listed in Table 3. The result shows that the uniformity of the temperature is significantly improved through the optimization. After the first level optimization (M2), the maximum temperature difference of the cooling air is decreased from 23.9 K to 10.1 K. The temperatures in the front passages and the rear passages are slightly higher than those in the middle passages. After the second level and the third level optimization (M3 and M4), the maximum temperature differences of the cooling air are decreased to 4.9 K and 2.1 K, respectively. The distribution

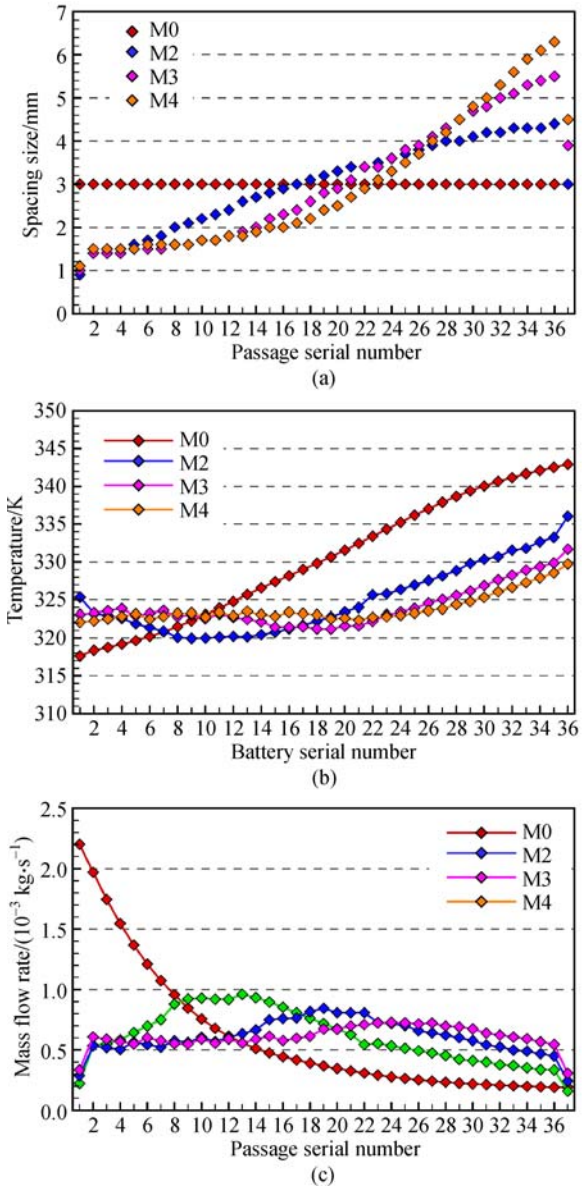

Fig. 8 Distributions of the (a) passage spacing size, (b) maximum temperature on the battery cell, and (c) passage mass flow rate for M0, M2, M3, and M4

of the passage mass flow rate (as shown in Fig. 8(c)) also tends to be even except the first and the last passage due to only one side of the battery cell heating the cooling air.

It is also seen from Table 3 that the temperature uniformity among the battery cells is relatively worse than the uniformity of the air. When the maximum temperature difference of the cooling air reaches to 2.1 K in M4, the maximum temperature difference on the battery cells is still 7.6 K. A pressure drop increment of 18 Pa is observed after optimization, and the pressure drop is relatively stable from Case M2 to Case M4.

In order to improve the temperature uniformity among the battery cells, an additional case M5 is conducted.

Table 3 Maximum temperature difference of the cooling air among the passages (ΔT_{amax}), maximum temperature difference among the battery cells (ΔT_{max}), and pressure drop in different cases

Case	ΔT_{amax} /K	ΔT_{max}/K	Pressure drop/Pa
M0	23.9	25.3	212.08
M1	85.4	100.6	245.35
M2	10.1	16.1	229.37
M3	4.9	10.5	230.82
M4	2.1	7.6	229.43

Though the heat is taken away by the cooling air, it needs to be transferred from the battery cell to the cooling air. In M5, the input parameters of the temperature difference of the cooling air between the outlet and inlet of each passage (ΔT_{ai}) in Eq. (11) are replaced by the maximum temperature on the battery cell that is extracted from M4. Figures 9(a) and 9(b) show the distributions of passage spacing size, the passage mass flow rate, the air temperature at different passage outlet, and the maximum temperature on the battery cell. Compared to M4, the maximum temperature on the battery cell in M5 is increased on the front battery cells and decreased on the rear battery cells. However, this difference is small, especially in the rear passages. And the maximum temperature difference among the battery cells is decreased by 6.4 K compared to 7.6 K in M4. Another interesting finding is that even if the passage mass flow rate in the rear passages is larger than that in the front passages, the maximum temperature on the battery cell in the rear battery cells is still higher. It is seen from Fig. 9 that the passage mass flow rate is increased by the large passage spacing size. However, due to the large flow area, the velocity magnitudes in the rear passages are still very small. Thus, the heat transfer between the wall and the cooling air is low; the heat transfer between the cooling air near the wall and the cooling air in the center of the passage is also small. The temperature contours in the rear passages are shown in Fig. 9(c). It is observed that in the rear passages, the temperature of the cooling air in the center of the passage is significantly lower than that near the wall.

5 Conclusions

This paper designed and optimized an air-based BTMS in electric vehicles. A sensitivity analysis was performed to study the effects of three key parameters on the thermal performance, i.e., the mass flow rate of the cooling air, the heat flux from the battery to the air, and the passage spacing size. The metrics of the temperature uniformity in the battery module and the pressure drop were used to evaluate the thermal performance. This sensitivity analysis showed that:

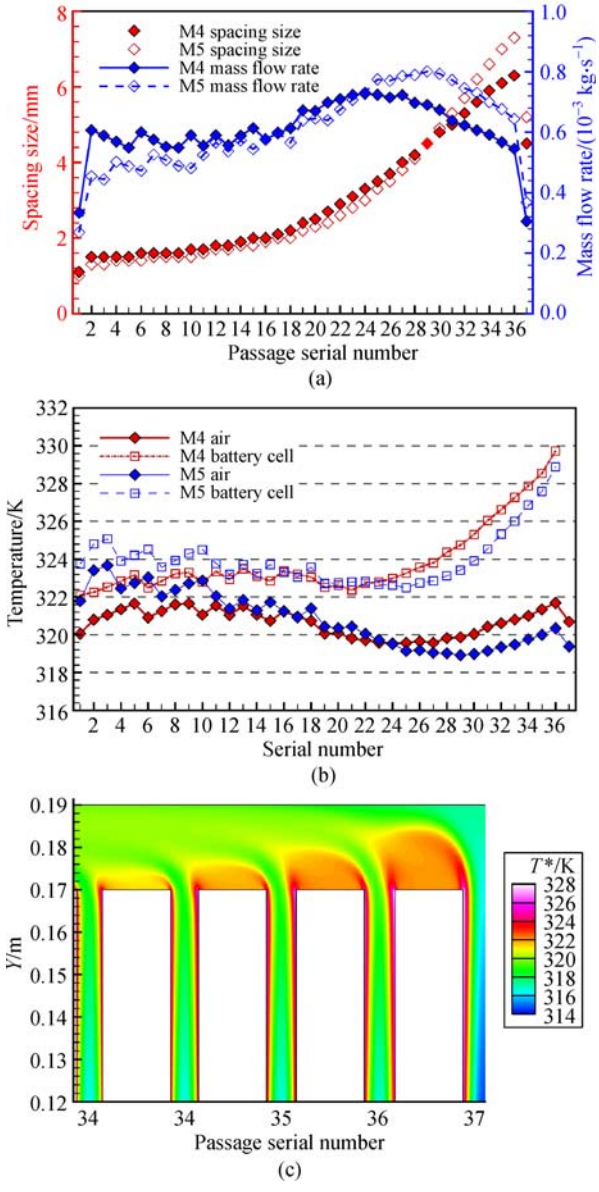

Fig. 9 Distributions of the (a) passage spacing size and passage mass flow rate, (b) the air temperature at the passage outlet and the maximum temperature on the battery cell for M4 and M5, and (c) temperature contours in the rear passages in M5

• Increasing the total mass flow rate could reduce the maximum temperature but also increase the pressure drop, thereby resulting in a more nonuniform distribution of the passage mass flow rate among passages.

• The heat flux significantly affected the maximum temperature on the battery cell, and had less effect on the pressure drop and the distribution of the passage mass flow rate. A large heat flux might result in a worse thermal environment, especially for the rear battery cells.

• A large passage spacing size might worsen the temperature uniformity among the battery cells. When the passage spacing size was large, most of the cooling air came through the front passages, which caused the lack of the cooling air in the rear passages. Therefore, the temperatures on the battery walls were very high.

To improve the performance of the air-based cooling system, the passage spacing size was optimized, with constant mass flow rate, heat flux, and total battery module length. Optimization results showed that:

• When the passage spacing size was small, the boundary layer effect that significantly affected the velocity that should be considered in the optimization.

• When the passage spacing size is optimized based on the air density, velocity, and air temperature, the temperature uniformity of the cooling air was significantly improved. The maximum temperature difference of the cooling air was reduced from 23.9 K to 2.1 K.

• After the optimization, the temperature uniformity among the battery cells was relatively worse than the uniformity of the air temperature among the passages, due to the low velocity of the cooling air. Using the maximum temperature on the battery cell as the input parameter, the maximum temperature difference among the battery cells was reduced to 6.4 K.

In the studied battery module, since the inlet and outlet are on the same side, the small pressure difference between the inlet and outlet in the rear passages is unavoidable. In future work, the passage spacing size and the position of the inlet/or the outlet, and the configuration of the manifold will be optimized simultaneously.

Acknowledgements This work was supported by the University of Texas at Dallas. The author of Mao Li and Xiaobang Wang were supported by the China Scholarship Council.

References

1. Kizilel R, Sabbah R, Selman J R, et al. An alternative cooling system to enhance the safety of Li-ion battery packs. Journal of Power Sources, 2009, 194(2): 1105–1112
2. Lu L, Han X, Li J, et al. A review on the key issues for lithium-ion battery management in electric vehicles. Journal of Power Sources, 2013, 226(3): 272–288
3. Rao Z, Wang S. A review of power battery thermal energy management. Renewable & Sustainable Energy Reviews, 2011, 15 (9): 4554–4571
4. Fotouhi A, Auger D J, Propp K, et al. A review on electric vehicle battery modelling: From lithium-ion toward lithium-sulphur. Renewable & Sustainable Energy Reviews, 2016, 56: 1008–1021
5. Ling Z, Zhang Z, Shi G, et al. Review on thermal management systems using phase change materials for electronic components, Li-ion batteries and photovoltaic modules. Renewable & Sustainable Energy Reviews, 2014, 31(2): 427–438
6. Zhao R, Zhang S, Liu J, et al. A review of thermal performance improving methods of lithium ion battery: Electrode modification and thermal management system. Journal of Power Sources, 2015, 299: 557–577
7. Park H. A design of air flow configuration for cooling lithium ion

battery in hybrid electric vehicles. Journal of Power Sources, 2013, 239: 30–36
8. Giuliano M R, Prasad A K, Advani S G. Experimental study of an air-cooled thermal management system for high capacity lithium-titanate batteries. Journal of Power Sources, 2012, 216(216): 345–352
9. Rao Z, Wang Q, Huang C. Investigation of the thermal performance of phase change material/mini-channel coupled battery thermal management system. Applied Energy, 2016, 164: 659–669
10. Huo Y, Rao Z, Liu X, et al. Investigation of power battery thermal management by using mini-channel cold plate. Energy Conversion and Management, 2015, 89: 387–395
11. Jarrett A, Kim I Y. Influence of operating conditions on the optimum design of electric vehicle battery cooling plates. Journal of Power Sources, 2014, 245(1): 644–655
12. Liu R, Chen J, Xun J, et al. Numerical investigation of thermal behaviors in lithium-ion battery stack discharge. Applied Energy, 2014, 132(11): 288–297
13. Greco A, Cao D, Jiang X, et al. A theoretical and computational study of lithium-ion battery thermal management for electric vehicles using heat pipes. Journal of Power Sources, 2014, 257(3): 344–355
14. Ye Y, Saw L H, Shi Y, et al. Numerical analyses on optimizing a heat pipe thermal management system for lithium-ion batteries during fast charging. Applied Thermal Engineering, 2015, 86: 281–291
15. Qu Z G, Li W Q, Tao W Q. Numerical model of the passive thermal management system for high-power lithium ion battery by using porous metal foam saturated with phase change material. International Journal of Hydrogen Energy, 2014, 39(8): 3904–3913
16. Li W, Qu Z, He Y, et al. Experimental study of a passive thermal management system for high-powered lithium ion batteries using porous metal foam saturated with phase change materials. Journal of Power Sources, 2014, 255: 9–15
17. Basu S, Hariharan K S, Kolake S M, et al. Coupled electrochemical thermal modelling of a novel Li-ion battery pack thermal management system. Applied Energy, 2016, 181: 1–13
18. Hwang H Y, Chen Y S, Chen J S. Optimizing the heat dissipation of an electric vehicle battery pack. Advances in Mechanical Engineering, 2015, 7(1): 204131
19. Fan L, Khodadadi J M, Pesaran A A. A parametric study on thermal management of an air-cooled lithium-ion battery module for plug-in hybrid electric vehicles. Journal of Power Sources, 2013, 238: 301–312
20. Zhao J, Rao Z, Huo Y, et al. Thermal management of cylindrical power battery module for extending the life of new energy electric vehicles. Applied Thermal Engineering, 2015, 85: 33–43
21. Xun J, Liu R, Jiao K. Numerical and analytical modeling of lithium ion battery thermal behaviors with different cooling designs. Journal of Power Sources, 2013, 233: 47–61
22. Ji B, Song X G, Cao W P, et al. Active temperature control of Li-ion batteries in electric vehicles. In: Proceedings of Hybrid and Electric Vehicles Conference (HEVC 2013). London: IEEE, 2013
23. Sun H, Wang X, Tossan B, et al. Three-dimensional thermal modeling of a lithium-ion battery pack. Journal of Power Sources, 2012, 206(206): 349–356
24. Sun H, Dixon R. Development of cooling strategy for an air cooled lithium-ion battery pack. Journal of Power Sources, 2014, 272: 404–414
25. Mohammadian S K, Zhang Y. Thermal management optimization of an air-cooled Li-ion battery module using pin-fin heat sinks for hybrid electric vehicles. Journal of Power Sources, 2015, 273(273): 431–439
26. Ling Z, Wang F, Fang X, et al. A hybrid thermal management system for lithium ion batteries combining phase change materials with forced-air cooling. Applied Energy, 2015, 148: 403–409
27. Yu K, Yang X, Cheng Y, et al. Thermal analysis and two-directional air flow thermal management for lithium-ion battery pack. Journal of Power Sources, 2014, 270(4): 193–200
28. Wang Z P, Liu P, Wang L F. Analysis on the capacity degradation mechanism of a series lithium-ion power battery pack based on inconsistency of capacity. Chinese Physics B, 2013, 22(8): 088801
29. Vetter J, Novák P, Wagner M R, et al. Ageing mechanisms in lithium-ion batteries. Journal of Power Sources, 2005, 147(1–2): 269–281
30. Zhu C, Li X, Song L, et al. Development of a theoretically based thermal model for lithium ion battery pack. Journal of Power Sources, 2013, 223(1): 155–164